Journal of Fluids and Structures (1997) **11,** 159–181

FLUIDELASTIC INSTABILITY IN A TUBE ARRAY SUBJECTED TO PARTIAL ADMISSION WATER CROSS-FLOW

J. L. PARRONDO AND C. SANTOLARIA
Departamento de Energía, Universidad de Oviedo, Gijón, Spain
AND
D. S. WEAVER
Department of Mechanical Engineering, McMaster University, Hamilton, Canada

(Received 18 December 1995 and in revised form 18 July 1996)

An experimental investigation of the critical conditions for fluidelastic instability is presented for a parallel triangular tube array with a pitch-to-diameter ratio of 1·57. The array was subjected to water cross-flow with partial admission and 10 test series were conducted with different support locations along the tubes, in order to vary their natural frequencies and mode shapes. In this way, the influence of cross-flow with partial admission, as a particular case of nonuniform cross-flow, could be studied systematically. A variety of the response curves obtained apparently exhibit more than one critical flow velocity for each mode of vibration, so that when representing all the data in a stability map, up to three instability regions are shown for the lower range of the mass-damping parameter. However, the low vibration amplitudes observed for the lower two regions suggest that they may not be of practical importance in engineering practice. The data obtained are compared to stability boundaries proposed in the technical literature.

1. INTRODUCTION

BUNDLES OF TUBES SUBJECTED TO CROSS-FLOW may vibrate due to a number of different excitation mechanisms, usually classified as turbulence buffeting, vortex shedding (with structural or acoustic resonance) and fluidelastic instability (Weaver & Fitzpatrick 1988). The latter is recognized to be the mechanism most likely to cause industrial heat exchanger tube damage and it is characterized by the development of large amplitude oscillations, at one of the low natural frequencies of the tubes, when the cross-flow velocity exceeds a certain critical value. The exact nature of the instability mechanism, however, may vary from case to case depending on the array geometry and fluid. Researchers usually distinguish between damping-controlled or stiffness-controlled mechanisms, which require one or more than one degree of freedom, respectively (Chen 1983; Païdoussis & Price 1988).

Although a number of theoretical models have been proposed to explain the phenomenon (Price 1995), the design of heat exchangers against fluidelastic instability continues to be based on correlations of laboratory data. A general expression for these correlations is

$$\frac{V}{fd} = K\left(\frac{m\delta}{\rho d^2}\right)^{\alpha}, \tag{1}$$

where V is the critical velocity, f, the frequency of vibration, d, the outside diameter of the tubes, m, the mass of the tubes per unit length (including added mass), ρ, the fluid

0889–9746/97/020159 + 23 $25.00/fl960071

density, and δ, the logarithmic decrement of damping of the tubes. The ratio $m\delta/(\rho d^2)$ is usually referred to as the mass-damping parameter. The most commonly used correlations assume $\alpha = 0{\cdot}5$ (Pettigrew & Taylor 1991), in agreement with Connors' (1970) theory.

The use of equation (1) is restricted to cases with uniform flow across the total length of the tubes. Tube arrays of real heat exchangers have multi-span tubes subjected to nonuniform cross-flow, with distribution $V\psi(x)$, and for this practical case, equation (1) with $\alpha = 0{\cdot}5$ was extended theoretically (Franklin & Soper 1977; Blevins 1977; Connors 1978; Pettigrew *et al.* 1978) to give

$$\frac{V_i}{f_i d} = K\left[\frac{m\delta_i}{\rho d^2}\frac{\int_0^l \phi_i^2(x)\,\mathrm{d}x}{\int_0^l \psi^2(x)\phi_i^2(x)\,\mathrm{d}x}\right]^{\frac{1}{2}}, \tag{2}$$

where subscript i refers to the ith mode of vibration of the tubes and $\phi_i(x)$ is the corresponding mode shape function.

Recent wind tunnel investigations on multi-span tube arrays (Waring & Weaver 1988; Weaver & Goyder 1990; Weaver & Parrondo 1991) showed that, in many cases, equation (2) provides a reasonable engineering approximation. However, Weaver & Parrondo (1991) also tested a number of cases with partial admission (uniform flow across only one span of the tubes and no flow on the rest) for which equation (2) either failed to predict the critical modes observed or gave critical velocity predictions that were up to 70% unconservative when using coefficient $K = 3{\cdot}3$ (and V the pitch velocity). Weaver & Parrondo suggested an alternative design expression that always gave the correct mode predictions, even when equation (2) failed, namely

$$\frac{V_i}{f_i d} = K\left(\frac{m\delta_i}{\rho d^2 S_i}\right)^{\alpha}, \tag{3}$$

$$S_i = \frac{\int_{l_1}^{l_2} \phi_i^2(x)\,\mathrm{d}x}{\int_0^l \phi_i^2(x)\,\mathrm{d}x}, \tag{4}$$

where l_1 and l_2 are the limits of the span subjected to cross-flow and K and α depend on the array geometry. Equation (3) is just the extension of equation (1) to the case of uniform cross-flow with partial admission on the tubes (Weaver & Goyder 1990) and in such case, if $\alpha = 0{\cdot}5$, equation (3) reduces to equation (2). S_i is called the energy fraction since it represents the ratio of the kinetic energy of the span subjected to uniform cross-flow to that of the whole tube. The values used for α and K were those proposed by Weaver & Fitzpatrick (1988) for each different array geometry, based on an empirical fit of the data reported in the technical literature. In particular, the exponent α recommended by these authors was always less than 0·5, although it was close to 0·5 for square and rotated square arrays.

For the low range of the mass-damping parameter (water cross-flow) the experimental data available in the literature are sparse and virtually restricted to the case of uniform cross-flow. However these data suggest that the reduced critical velocity for fluidelastic instability is essentially independent of the mass-damping parameter for values of the latter less than about 0·3 (Weaver & Yeung 1984; Weaver & Fitzpatrick 1988). Additionally, for these low values of the mass-damping parameter, some of the

theoretical models proposed for fluidelastic instability, such as those due to Lever & Weaver (1982), Chen (1983) or Price & Païdoussis (1986), predict the existence of multiple instability regions, i.e., more than one critical velocity for each value of the mass-damping parameter. In fact, Chen & Jendrzejczyk (1983) reported a stability map with a secondary instability region (two critical velocities), obtained from tests on a single row of tubes subjected to water cross-flow. More recently Andjelić *et al.* (1992), who conducted wind tunnel experiments on a normal triangular tube array with a pitch-to-diameter ratio of 1·25 and with variable damping, obtained a stability map with three critical velocities for each value of the mass-damping parameter. On the other hand, Païdoussis *et al.* (1995) have argued that the multiple stability regions have no practical significance.

The above discussion indicates that tube arrays subjected to a cross-flow of heavier fluids such as water show different stability behaviour than those operating at higher mass-damping parameters. Additionally, equation (2) is commonly used to extend stability data obtained from uniform flows to cases of nonuniform flow distributions, and there exists no published data which validates such an extension for low mass-damping parameter arrays. The purpose of the research reported in this paper was to overcome these deficiencies. Water tunnel results are presented for the fluidelastic instability of a parallel triangular tube array with a pitch-to-diameter ratio of 1·574. The tubes were subjected to a water cross-flow with partial admission, i.e. there was uniform flow across a portion of their total length, while the remaining portion was immersed in still water. Tests were conducted with different support locations along the tubes, thus varying their natural frequencies and mode shape functions, in order to study the influence of the nonuniform cross-flow distribution on the critical conditions for fluidelastic instability. The results obtained are compared to the stability boundaries of design criteria proposed in the literature.

2. EXPERIMENTAL EQUIPMENT

The water tunnel facility used for this investigation is shown schematically in Figure 1. The flow was provided by a centrifugal pump driven by a 50 kW motor with speed regulated by a frequency controller. The flow was passed through a settling chamber followed by a nozzle with a contraction ratio of 9:1, so that a flat velocity profile was obtained at the entrance of the test-section for any flow rate. The acrylic test-section was 68 mm wide and 200 mm high (internal dimensions). Transmission of vibrations from the pumping system to the test-section was avoided by using flexible hoses in the ducts.

The tube bundle tested was a parallel triangular array with a pitch-to-diameter ratio of 1·574 and six rows of tubes. The tubes were brass with an outside diameter of 10 mm and 0·5 mm wall thickness. There were 12 flexible tubes that filled the four central columns of the array (Figure 2). A 10 mm inside-diameter ring with exterior thread was welded at one end of each flexible tube, so that these tubes could be screwed into a 30 mm thick brass plate, provided with suitable holes that followed the pattern of the array. In this way the tubes could be considered clamped at the plate, with a 0·679 m cantilever length from the clamping point (Figure 3). The array was completed with six half-tubes as shown in Figure 2. One end of these half-tubes was welded to the plate where the flexible tubes were screwed, and the other end was welded to another 20 mm thick brass plate with a window large enough for the flexible tubes to pass through without contact.

The assembly formed by the plates and the half-tubes could be inserted through and

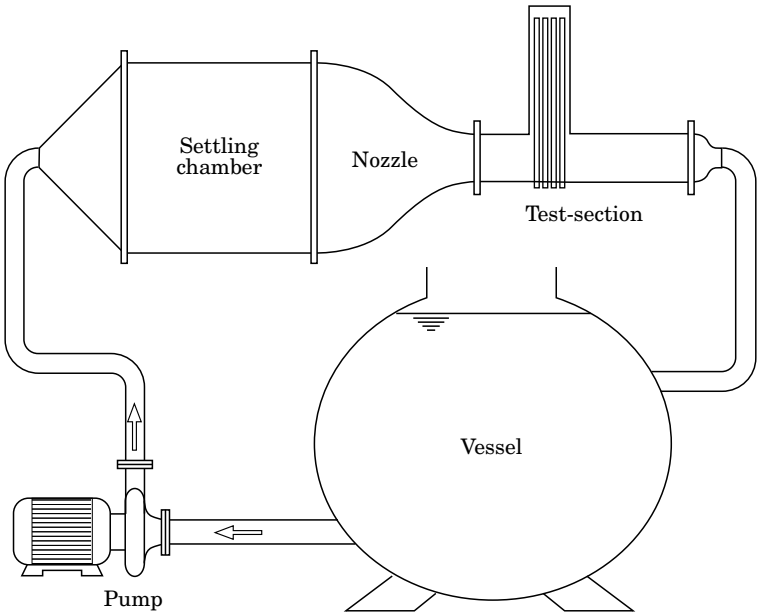

Figure 1. Schematic of the water tunnel facility.

fixed at the bottom surface of the working section, so that water could not leak and the flexible tubes could easily be instrumented from the outside of the test-section. The tube bundle was mounted vertically in the test-section and was subjected to a uniform water cross-flow along 200 mm starting at 20 mm over the clamping point (Figure 3). The test-section had a prismatic chamber on the upper side so that the span of the tubes that was not subjected to water cross-flow was immersed in still water. The mass

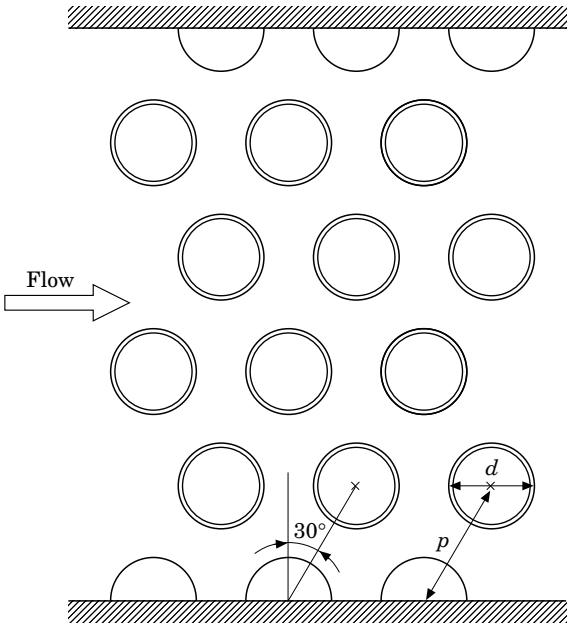

Figure 2. Cross section of the tube array ($d = 10$ mm, $p = 15{\cdot}7$ mm).

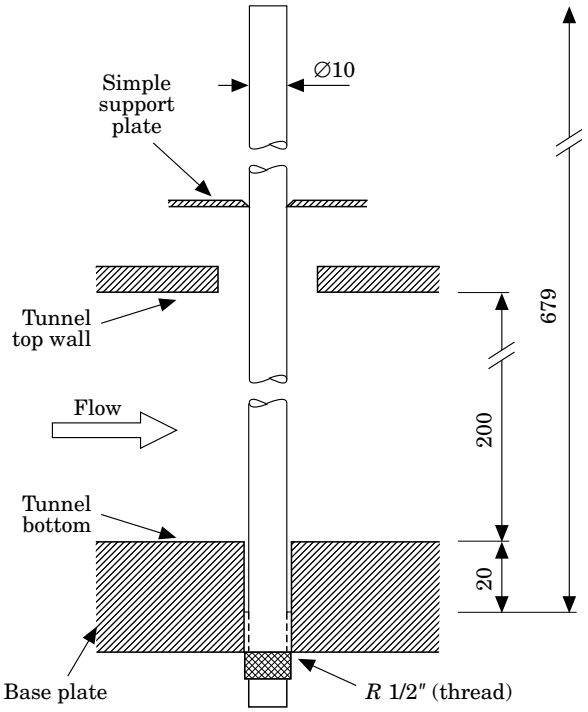

Figure 3. Schematic of the mounting of the tubes in the test section (dimensions in mm).

ratio between tubes and water was $m_A/\rho d^2 = 1{\cdot}26$, where m_A is the mass per unit length of the tubes without inclusion of the added mass.

Additionally, another thin brass plate was made which had 10 mm diameter holes cut in the array pattern with an edge width of 0·5 mm, in order to provide a simple support for the tubes. That plate could be rigidly fixed at the walls of the prismatic chamber, at any position along the tubes. Experiments were done on nine different positions of the simple support plate, plus another case for which the tubes were cantilevered. The ten configurations tested are listed in Table 1.

TABLE 1

Characteristics of the tube array tested and measurements in still fluid

Test	l_1 (m)	l_2 (m)	1st mode frequency Air $f_{A,1}$ (Hz)	1st mode frequency Water $f_{W,1}$ (Hz)	Damping Log. dec. Air δ_A	Damping Log. dec. Water δ_W
A	0·0	0·679	14·1	10·8	0·007	0·080
B	0·271	0·408	30·2	23·0	0·008	0·089
C	0·286	0·393	31·5	23·4	0·016	0·120
D	0·317	0·362	35·5	27·7	0·011	0·060
E	0·401	0·278	52·7	40·8	0·015	0·063
F	0·526	0·153	87·5	65·5	0·007	0·069
G	0·557	0·122	85·4	64·8	0·018	0·104
H	0·592	0·087	80·0	64·0	0·011	0·084
I	0·617	0·062	74·1	55·2	0·015	0·071
J	0·666	0·013	64·4	49·0	0·008	0·078

For each test, one tube was instrumented with two Kulite GY-50 miniaccelerometers orthogonally mounted in a nylon carrier, which could be introduced into the tube from the outside of the test-section as explained above. They were oriented so that one of them measured the vibrations streamwise and the other one in the transverse direction. The acceleration signals were processed with a HP-3562A two-channel dynamic signal analyzer, which calculated their averaged r.m.s. spectra and permitted integration to obtain displacements. The approach flow velocity was measured with a pitot-static probe located 0·15 m upstream of the tube bundle, which could be connected either to a Validyne DP15 differential pressure transducer or to an inclined manometer with mercury, depending on the pressure range. The error estimated for the flow velocity measurements was less than 2·5% for velocities greater than 0·5 m/s.

A preliminary series of tests was conducted to check on the nature of the vibrations of the tubes. A Kistler 601A miniature piezoelectric pressure transducer was introduced into one of the tubes, in a way similar to that of the accelerometers, and it was located close to a 0·5 mm diameter hole, so that the fluctuations of the pressure acting on the tube at the position of the hole could be measured and recorded (Parrondo 1992). First, all the flexible tubes of the array were attached to one another and to the internal walls of the test-section, so that they could be considered effectively rigid. It was found that in such a case, and for different positions and orientations of the tube that contained the pressure transducer, no significant peaks were observed in the pressure spectra over the entire range of flow velocities, which would have suggested the existence of a forced excitation in the flow associated with a constant Strouhal number. Thus, apart from response due to broad band turbulent buffeting, any peaks in the response curves of the flexible tubes can be interpreted as being self-excited, i.e. due to fluidelastic instability (Parrondo 1992). This does not exclude, however, the possibility of vortex-shedding activity induced by the oscillation of the tubes once they are set into motion. Further discussion is presented in Section 4.2.

3. EXPERIMENTAL PROCEDURE AND RESULTS

3.1. Measurements in Still Fluid

Prior to each test, one tube of the third or fourth row was selected for monitoring. First, damping values of that tube were obtained by measuring the amplitude decay of the tube response after a small disturbance, both in still air and still water. To avoid modulations in the time response (Weaver & Koroyannakis 1982; Weaver & Yeung 1984), damping measurements in water were obtained while keeping rigid all the tubes except the one being monitored. It was found that this procedure usually gave damping values within 15% of the ones obtained with the complete array being flexible, when comparing the amplitudes of the signal at the maximum value of consecutive modulations. Damping values could be reliably obtained only for the first mode of vibration of the tubes. It should be noted that it is notoriously difficult to measure damping in tube bundles, especially in the higher modes, because of coupling between the tubes. This difficulty is aggravated in liquids because the fluid not only couples tube motion but possesses a different added mass for each mode of relative tube motion. The result is that a single tube mode is associated with a band of fluid coupled mode frequencies. In a transient test of a flexible array, energy is transferred back and forth between tubes, producing significant modulations in amplitude decay. The higher modes disappear too quickly to obtain reliable damping data. Under external excitation, methods such as the half-power bandwidth of the frequency response

resonance peak are problematic because the underlying assumptions of a linear stationary response at a unique frequency are violated.

Table 1 summarizes the values of the logarithmic decrement of damping measured in both still air (δ_A) and water (δ_W) for each test (lift direction), together with the frequencies excited. The measured frequencies in still water were the same in the lift and drag directions within 3%. It is seen that damping values in water are about an order of magnitude greater than those in air. Also, the frequencies, f_W, excited in still water are about 25% smaller than the frequencies, f_A, excited in still air, due to the added mass. The corresponding added mass coefficients C_M may be calculated with the expression

$$C_M = \left[\left(\frac{f_A}{f_W}\right)^2 - 1\right]\frac{4m_A}{\rho\pi d^2}. \tag{5}$$

The average value of C_M obtained from the data of Table 1 is 1·18, with a standard deviation of 0·127. This value is close to 1·25, which is the value obtained from Moretti & Lowery's (1976) plot of added mass coefficient, measured for a triangular array of seven tubes, all rigid except the central one, with variable pitch-to-diameter ratio.

3.2. Tube Response as a Function of Flow Velocity

After the damping measurements were completed, the pump was run at progressively greater rotational speeds, from a sufficiently low value with no appreciable tube vibration up to a flow rate well above the stability threshold. At each flow velocity, the r.m.s. power spectral density of the acceleration in both the streamwise and the transverse direction were recorded (Figure 4). These spectra usually showed significant response in separate bands of frequencies, each of them being associated with a different mode of vibration. Each band contained one or more dominant peaks. When the flow velocity was increased, the dominant peaks shifted slightly towards higher

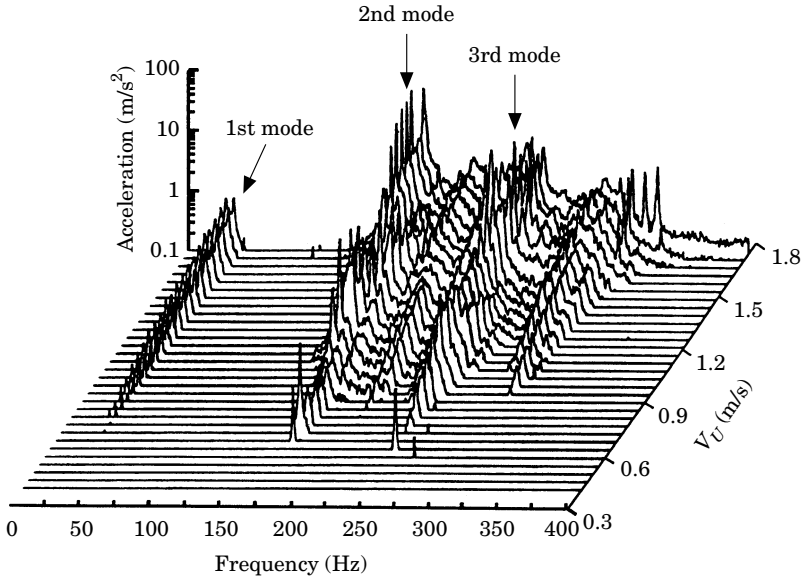

Figure 4. Variation of the power spectral density of the acceleration with the upstream velocity V_U of the cross-flow, for case D. The accelerometer was oriented in the cross-flow direction and positioned at 0·18 m from the tip of the tube.

frequencies and their amplitude did not vanish until they reached the upper limit of the associated band. By then, more peaks usually appeared at the lower limit of the band, which would subsequently follow the same process. This behaviour has been observed in other investigations (Weaver & Koroyannakis 1982). An especially relevant fact is that in no case was a constant ratio observed between the frequency of the shifting spikes and the flow velocity (i.e., a constant Strouhal number), not even for a short range of velocity, as would correspond to vorticity-type excitation. This supports the interpretation of the response of the tubes as instability, as mentioned above in Section 2.

Response curves were obtained by choosing the highest peak for each mode in the displacement power spectra, after vectorial summation of the twice integrated signal from each accelerometer. In general, the amplitudes of vibration in the streamwise and transverse directions were of the same order of magnitude, depending on the cross-flow velocity and on the frequency considered. Since the accelerometers were not located at the position of maximum displacement of the tube, this maximum displacement had to be obtained by using the appropriate shape functions for each mode and configuration. For this purpose, a computer program was developed to solve Euler's equation for the transverse vibrations of a beam with variable support conditions, including the effects of rotary inertia and shearing deformation, so that the natural frequencies and mode shape functions of the tubes could be calculated. The differences found between the frequencies predicted for the first mode and the frequencies measured with the tubes in air were always less than 1%. Calculations also showed that, at least for the first three modes of the tubes in the present study, the effects of transverse shear and rotary inertia are negligible, as might be expected. The mode shape functions in vacuum are not expected to be modified when the tubes are in still water, because in this case there is a uniform distribution of added mass along the tubes. However, this may not be true in general for multi-span tubes subjected to nonuniform cross-flow, due to the possible effect of the flow velocity on added mass. To check this, measurements were taken for support configuration A which consisted of varying the position of the accelerometers along the tubes while keeping a constant flow velocity. These tests showed that the distortion of the shape functions calculated for vacuum conditions could be considered negligible in the range of velocities of interest in this study.

3.3. Critical Velocities for Each Case Tested

Figures 5 to 14 show one of the response curves obtained for each position of the simple support plate, together with the mode shape functions calculated for the first three modes of vibration. For case A, the tubes were cantilevered, for case B the simple support plate was located 0·408 m from the free end of the tubes and, for the other cases, the support plate was progressively shifted towards the free end. It is important to remember that only the 200 mm portion of the tubes next to the base is exposed to cross-flow, regardless of the simple support plate location. Determination of the critical velocities from the response curves alone was not always straightforward and use was made of the acceleration spectra to assist in interpreting the results. In general, instability is considered to occur when the slope of the amplitude-velocity curve increases abruptly and the tube response becomes organized to a whirling pattern at a single frequency. Of course, this definition of critical velocity does not distinguish fluidelastic instability from vortex-shedding resonance as the cause of the peak. The latter cause is eliminated by other arguments as discussed earlier, in Section 2, and below in Section 4.2. Some brief explanations are given below for each case. In spite of the complexity of some of the response curves, good repeatability was found between

tests for a given case. Maximum differences between critical velocities were less than 5%, even when monitoring different tubes.

3.3.1. *Case A* (*Figure* 5)

The vibration amplitude for both the first and second modes increases slowly with the flow up to an upstream velocity of about 1 m/s. For higher cross-flow velocities the response curves become much steeper, which indicates the development of fluidelastic instability for both modes. Very high amplitudes are reached, as expected for cantilevered tubes. The second mode appears to become unstable at about 1·05 m/s, slightly before the first mode (1·09 m/s).

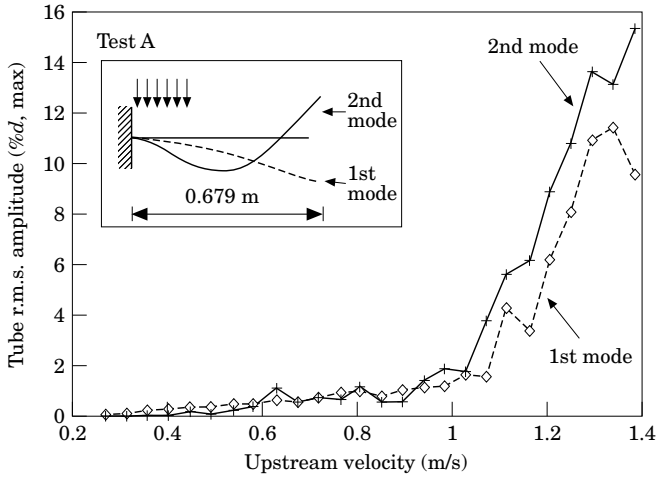

Figure 5. Response curves for test A.

3.3.2. *Case B* (*Figure* 6)

Very small response and no sign of instability was observed in the first mode (not presented) and the second mode for this configuration. However, though the maximum response amplitudes recorded for the third mode were small too (about 0·3% of the tube diameter), the evolution of the spectra and response curve suggests the development of instability for this mode. The critical velocity was estimated to be 1·72 m/s.

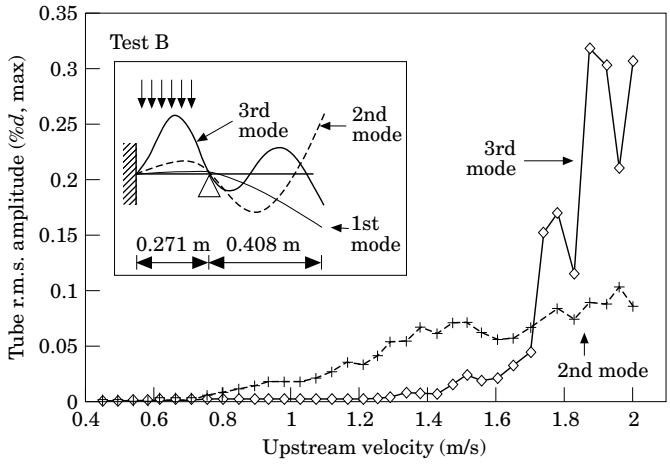

Figure 6. Response curves for test B.

3.3.3. *Case C* (*Figure* 7)
Similar to case B, no evidence of instability was observed in the first or second modes, whereas the third mode does appear to become unstable, though with very small response amplitude. However, this time the response curve presents at least two separate zones with relatively large amplitudes, which suggests the existence of multiple instability regions. The first one extends approximately between 1·07 m/s and 1·31 m/s. The second one starts at about 1·67 m/s and appears to be ending at about 2 m/s, though unfortunately the test was terminated before reaching that flow velocity.

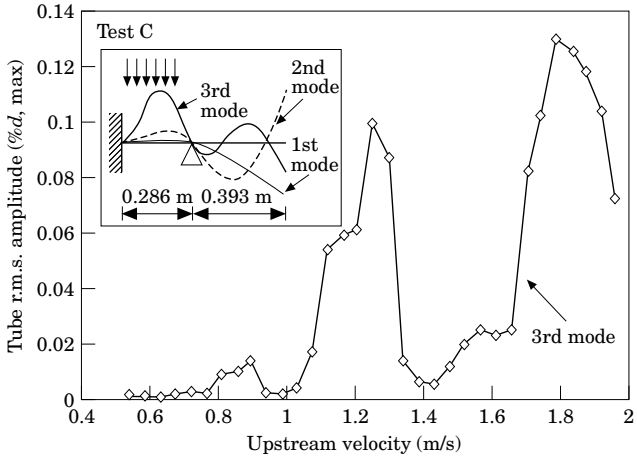

Figure 7. Response curves for test C.

3.3.4. *Case D* (*Figure* 8)
Whereas the first mode remains stable in the range of flows tested, the second mode becomes unstable at a velocity of about 1·73 m/s, reaching vibration amplitudes close to 5% of the tube diameter. The response for the higher modes was always small, but again a closer analysis of the third mode shows the possible development of instability too, at about 1·43 m/s. Finally some persistent spikes were observed in the second mode frequency region of the acceleration spectra recorded (Figure 4), in the range of velocities from about 0·65 to 0·71 m/s and afterwards from 1·0 to 1·32 m/s. Though the response amplitudes associated are small (about 0·2% of the tube diameter), they may possibly be considered as secondary instability regions for that mode.

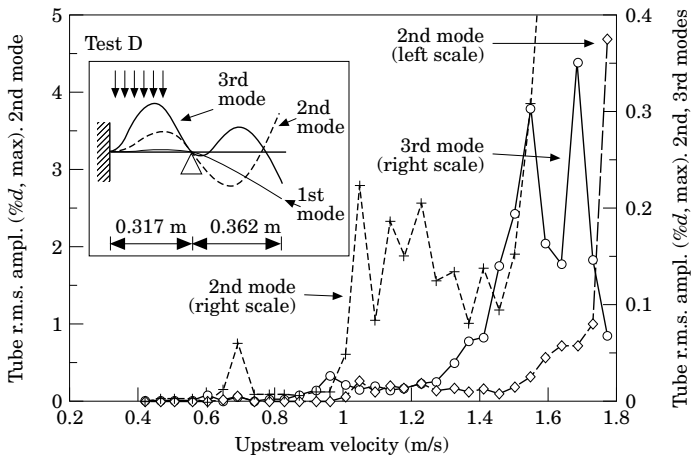

Figure 8. Response curves for test D.

3.3.5. *Case E* (*Figure* 9)

In this case the instability was also observed in the second and third modes. The second mode response shows relatively large amplitudes (up to 1% of the tube diameter) starting at about 0·88 m/s, but they drop off significantly at a velocity of about 1·2 m/s. At that velocity the third mode is the one to become apparently unstable, though with much smaller oscillation amplitudes (less than 0·1% of the tube diameter). Finally, the second mode shows a small peak in the region of 0·6 m/s.

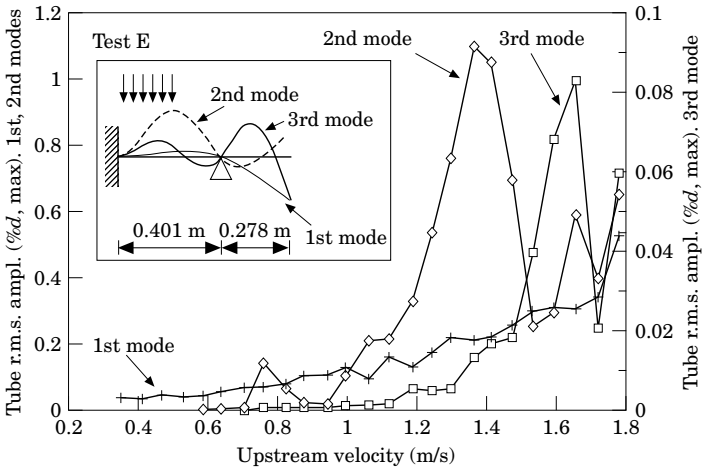

Figure 9. Response curves for test E.

3.3.6. *Case F* (*Figure* 10)

No significant response was observed except for the first mode. Its response curve clearly shows the development of large amplitude oscillations (up to 18% of the tube diameter at their free end) starting at an upstream velocity of 1 m/s. Also, some response in the first mode (1·5% of the tube diameter) is observed between about 0·78 and 0·9 m/s, which suggests the possible existence of a secondary unstable region.

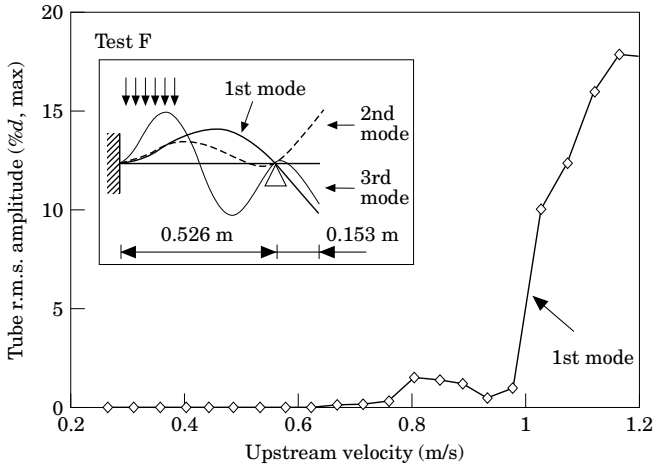

Figure 10. Response curves for test F.

3.3.7. *Case G* (*Figure* 11)

The first mode response looks much like that of case F. The first mode exhibits a clear peak in the range of velocities between 0·78 and 0·87 (the amplitude exceeds 3% of the tube diameter). For higher velocities the amplitude becomes very small again and finally large oscillations are developed from about 1·31 m/s. However in this case, the second mode apparently becomes unstable as well. This is suggested by the sharp increase in response amplitude, at about 1·1 m/s, in spite of the relatively small maximum amplitude levels (0·6% of the tube diameter).

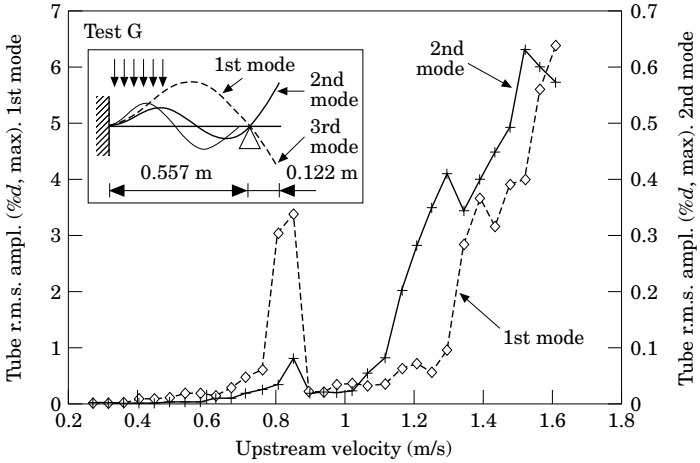

Figure 11. Response curves for test G.

3.3.8. *Case H* (*Figure* 12)

A very similar behaviour is observed for this case. The first mode develops significant oscillations from an upstream velocity of about 0·65 to 0·78 m/s. Large oscillations are also observed at higher flows; the corresponding critical velocity was estimated at about 1·27 m/s. Second mode amplitudes are small (less than 0·5% of the tube diameter), but the response curve and acceleration spectra recorded suggest the development of instability at about 1·07 m/s.

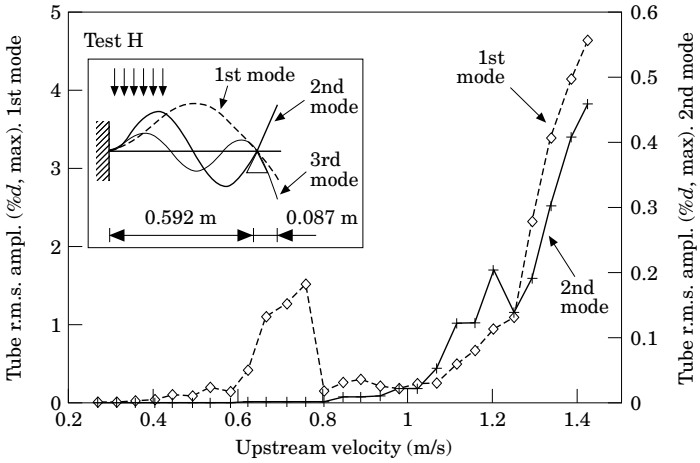

Figure 12. Response curves for test H.

3.3.9. *Case I* (*Figure* 13)

In this case both the first and the second modes were found to become unstable. The first mode is seen to become unstable at a critical velocity of about 1·28 m/s, reaching amplitude values of over 3% of the tube diameter. At higher flows, coinciding with a decrease in the first mode response, the second mode develops instability. Though the greatest oscillations (3% of the tube diameter) are not reached till about 2·1 m/s, the corresponding critical velocity is estimated to be 1·81 m/s, after analysis of the acceleration spectra. Also, the second mode response apparently presents a secondary instability region, with amplitudes up to 1% of the tube diameter in the flow velocity range between 1·09 and 1·34 m/s.

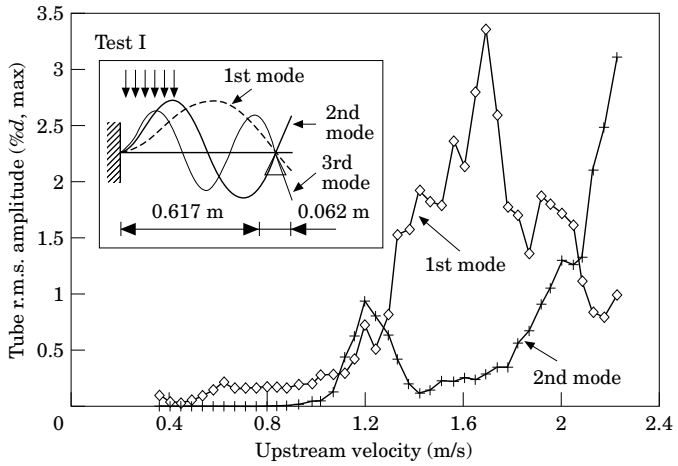

Figure 13. Response curves for test I.

3.3.10. *Case J* (*Figure* 14)

In this case the behaviour is similar to that for case I. The first mode becomes unstable at a critical velocity of about 1·18 m/s. The second mode becomes unstable too, at a critical velocity of about 1·48 m/s. Additionally, the second mode shows a possible secondary instability region (oscillations of about 0·5% of the tube diameter), approximately between 0·95 m/s and 1·09 m/s.

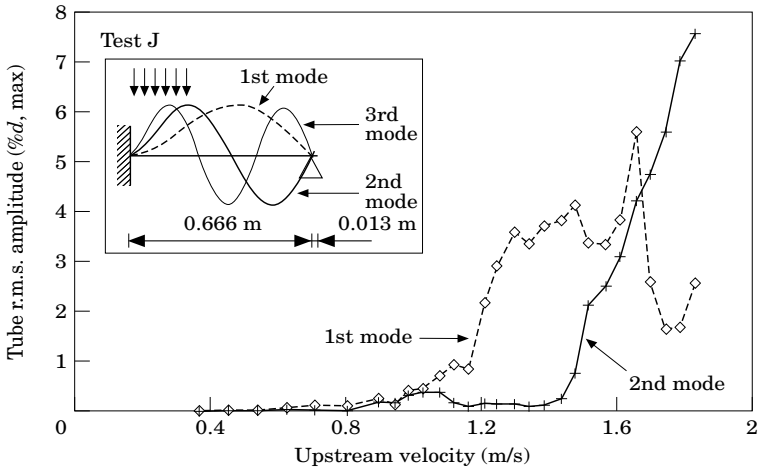

Figure 14. Response curves for test J.

3.3.11. *General discussion of Cases A–J*

To sum up, a number of the test cases were found to exhibit more that one clear peak in the response curves which could be interpreted as multiple regions of instability. Table 2 presents a summary of the upstream critical velocities established for each case and mode, including those corresponding to possible secondary instability regions. The vibration frequencies associated with each critical velocity are also included, together with a reference number (from 1 to 36). The data were classified in three groups,

TABLE 2

Upstream critical velocities V_U and frequency f at instability for each test

Group*	Test	Mode	V_U (m/s)	f (Hz)	Ref.**
1	A	1	1·09	12·1	1
	A	2	1·05	71·4	2
	D	2	1·73	167·0	3
	F	1	1·00	64·3	4
	G	1	0·78	63·9	5
	G	1	1·31	59·8	6
	H	1	1·27	56·3	7
	I	1	1·28	58·1	8
	I	2	1·81	175·5	9
	J	1	1·18	47·2	10
	J	2	1·48	140·3	11
2	B	3	1·72	282·0	12
	D	3	1·43	235·0	13
	E	2	0·88	142·0	14
	F	1	0·78	64·5	15
	G	2	1·10	161·5	16
	H	1	0·65	57·0	17
	H	2	1·07	171·0	18
	I	2	1·09	160·3	19
	J	2	0·95	141·8	20
3	C	3	1·07	285·0	21
	C	3	1·67	280·0	22
	D	2	0·65	168·0	23
	D	2	1·02	164·5	24
	E	2	0·60	145·5	25
	E	3	1·17	311·0	26
4	C	3	1·31	296·0	27
	D	2	0·71	170·0	28
	D	2	1·32	180·8	29
	E	2	0·67	147·0	30
	E	2	1·17	149·0	31
	F	1	0·90	65·7	32
	G	1	0·87	65·9	33
	H	1	0·78	59·5	34
	I	2	1·34	165·4	35
	J	2	1·09	141·6	36

* Group 1: $A > 2\%d$; Group 2: $0{\cdot}3\%d < A < 2\%d$; Group 3: $A < 0{\cdot}3\%d$; Group 4: ending limit of oscillations. A = maximum amplitude of oscillation; d = tube diameter.

** Reference numbers in Figures 15 and 16.

depending on the maximum response amplitude observed when increasing the cross-flow velocity from the critical value: group 1, amplitudes greater than 2% of the tube diameter; group 2, amplitudes between 0·3 and 2% of the tube diameter; and group 3, amplitudes less than 0·3% of the tube diameter. A fourth group gives the velocity at the upper limit of the apparent secondary instability regions. A detailed discussion of the possible interpretation of these response peaks and data groupings is left to the next section.

The frequencies excited at each stability threshold (lower limits only) were compared to the natural frequencies of the tubes in air by means of equation (5). The added mass coefficients so obtained showed a mean value of 1·45 with a standard deviation of 0·32 from a total of 26 data. The most discordant data were those of case A, which gave unexpectedly low added mass coefficients of 0·59 for the first mode and 0·72 for the second. When these two data were not included in the computation, the average value found was 1·55 with standard deviation of 0·20. Added mass coefficients were also calculated with respect to the lower limit of the band of frequencies associated with each mode of vibration in the acceleration spectra recorded. A total of 24 data led to a mean value of 1·93 with a standard deviation of 0·25. That mean value is close to a value of 2·0, which is the upper bound of the added mass coefficient as predicted by Chen's (1977) potential flow theory for an array of 19 cylinders in still fluid.

There is some question as to the validity of using equation (5) when the fluid is flowing because this assumes that the frequency reduction from the value in air is entirely due to fluid added mass, i.e., the possible effects of fluid stiffness are ignored and cannot be accounted for. While fluid stiffness may explain the low values of added mass observed for case A, it seems more likely that these are due to the nonlinear effects of large amplitude motions. In any event, the bulk of the experimental data show that a good estimate of the lowest observed tube frequency under flow conditions can be obtained by using the highest added mass coefficient computed from potential flow theory with the theoretical *in vacuo* tube natural frequency for a given mode.

4. STABILITY MAPS AND DISCUSSION

4.1. Plot of Data in Stability Maps

As mentioned above, typical design correlations against fluidelastic instability have the general expression shown in equation (1), which is valid for uniform flows across the total length of the tubes. In case of tubes with partial admission, such as the ones tested in this investigation, the appropriate design expression is given by equation (3). Equation (1) may be considered as the particular case of equation (3) when the energy fraction, S_i, equals unity. With this perspective, the data obtained from the present experiments may be plotted on a traditional stability map, using the critical reduced velocities and the mass-damping parameter divided by the energy fraction, which is subsequently called the mass-damping-energy fraction parameter, MDE (Parrondo *et al.* 1993). In this way, classical stability maps such as the ones presented by Weaver & Fitzpatrick (1988) are also valid for the case of tubes with partial admission, by considering the MDE parameter instead of the mass-damping parameter as the ordinate.

In order to obtain a stability map from the data measured, it was necessary to determine the values of the MDE parameter corresponding to each test. For this

purpose, the program used to obtain the natural frequencies and mode shapes of the tubes was augmented for evaluation of the energy fraction, given by equation (4). Two different MDE parameters were considered: one that used the damping values measured with the tubes in still air (MDE_A), and another one with the damping values measured in still water (MDE_W). In both cases the mass per unit length of the tubes was modified with an added mass coefficient $C_M = 1{\cdot}55$, which was the average value at critical conditions obtained from the present tests.

Since damping values had been measured only for the first mode of vibration of the tubes, damping values for the higher modes had to be estimated. The damping values measured in air (for MDE_A) were considered to be the same for all modes, because the damping added by the air is negligible and the structural and material components of the damping of structures may be reasonably assumed to be independent of the frequency. However, this is not so in the case of the liquid damping, which in fact was the most important component of damping with the tubes immersed in water (MDE_W). Neglecting the structural damping with respect to the damping added by water, and assuming the case of an isolated single tube vibrating in still fluid, with a constant drag coefficient and the same maximum amplitude of vibration for each mode, the damping $\delta_{W,i}$ corresponding to the ith mode of vibration may be determined (Blevins 1977) by

$$\frac{\delta_{W,i}}{\delta_{W,1}} = \frac{\int_0^l |\phi_i^3(x)|\,\mathrm{d}x \int_0^l \phi_1^2(x)\,\mathrm{d}x}{\int_0^l |\phi_1^3(x)|\,\mathrm{d}x \int_0^l \phi_i^2(x)\,\mathrm{d}x}. \tag{6}$$

To calculate the MDE_W parameters, equation (6) was used with $\delta_{W,1}$ equal to the damping values measured with the tubes in still water (see discussion in Section 3.1).

The values obtained for both MDE parameters, corresponding to the critical modes found in each test, are presented in Table 3. The critical velocity data are plotted in

TABLE 3

Calculated values of the natural frequency f_A, energy fraction S_i and mass-damping-energy fraction parameters MDE_A and MDE_W corresponding to the modes excited in each test

Case	Mode	f_A (Hz)	S_i	MDE_A	MDE_W
A	1	14·0	0·007	2·405	29·147
A	2	87·8	0·118	0·140	1·486
B	3	447·1	0·747	0·026	0·297
C	3	417·9	0·784	0·051	0·394
D	2	236·0	0·151	0·183	0·779
D	3	367·7	0·658	0·042	0·232
E	2	212·1	0·476	0·078	0·368
E	3	429·5	0·134	0·278	0·934
F	1	87·6	0·113	0·157	1·530
G	1	85·8	0·129	0·357	2·030
G	2	225·2	0·224	0·205	0·770
H	1	79·4	0·117	0·235	1·796
H	2	245·0	0·344	0·080	0·493
I	1	74·0	0·104	0·354	1·709
I	2	236·1	0·354	0·104	0·484
J	1	63·9	0·079	0·238	2·470
J	2	206·4	0·310	0·061	0·614

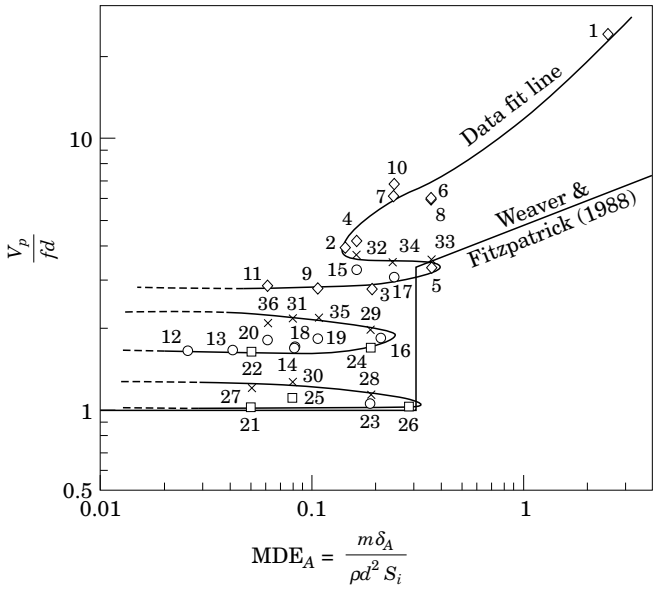

Figure 15. Stability map of the experimental data and comparison with the stability boundary of Weaver & Fitzpatrick (1988). Damping measured in air. ◇, Data from group 1 of Table 2; ○, data from group 2 of Table 2; □, data from group 3 of Table 2; ×, data from group 4 of Table 2.

Figures 15 and 16 against the MDE_A and the MDE_W parameters, respectively. Each data point is labelled with a reference number which permits identification from Table 2. In these graphs, the critical velocities are expressed in terms of the reduced pitch velocities $V_P/(fd)$, obtained with the expression

$$\frac{V_P}{fd} = \frac{p}{p-d}\frac{V_U}{fd} = 2{\cdot}74\,\frac{V_U}{fd}, \tag{7}$$

where V_P and V_U are the pitch and upstream velocities, f is the associated vibration frequency from Table 2, and p is the pitch of the array. Both stability plots look similar, as they are basically shifted one relative to the other by about one decade, due to the different definitions of damping used.

In both plots a curve has been drawn through the data, taking into consideration the critical velocities corresponding to the onset (Table 2, groups 1, 2 and 3) or to the disappearance (Table 2, group 4) of the response peak when increasing the cross-flow. Some scatter is observed in the data which might be attributed to experimental uncertainty but also to the slight changes in the relative positions between tubes that occur when varying the simple support location, which may have a significant effect according to the studies of Andjelić & Popp (1989) and Païdoussis *et al.* (1995). However both stability maps clearly show what may be considered as multiple instability regions for the lower range of the MDE parameter. Each secondary region is associated with a small range of the reduced critical pitch velocity ($1{\cdot}15 \pm 0{\cdot}1$, $1{\cdot}9 \pm 0{\cdot}25$ and $3{\cdot}3 \pm 0{\cdot}4$ respectively). It is important to note that the lower secondary region is primarily associated with the smallest response amplitudes (group 3 in Table 2), whereas the second region is associated primarily with data corresponding to intermediate response amplitude (group 2 in Table 2). The upper secondary loop, as well as the stability boundary for larger MDE parameters corresponds to large response amplitudes (group 1 in Table 3). Thus, each successive response region for

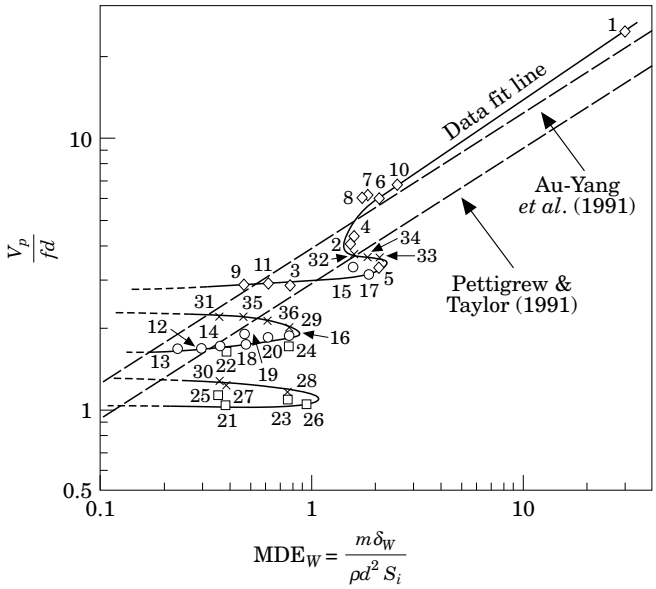

Figure 16. Stability map of the experimental data and comparison with the stability boundaries of Au-Yang *et al.* (1991) and Pettigrew & Taylor (1991). Damping measured in water. ◇, Data from group 1 of Table 2; ○, data from group 2 of Table 2; □, data from group 3 of Table 2; ×, data from group 4 of Table 2.

reducing critical velocity is generally associated with smaller response amplitudes. Such dependence between the response amplitude and the critical velocity associated with each region may explain why multiple regions have been so rarely documented in the technical literature. The interpretation of these observations is presented in the following section.

4.2. Discussion

The flow-induced response characteristics observed in these experiments and presented in the stability plots of Figures 15 and 16 could possibly be interpreted as multiple regions of instability at low values of the mass-damping parameter. The theoretical models of Lever & Weaver (1982) and Price & Païdoussis (1986) as well as subsequent versions reviewed by Price (1995) all predict the existence of multiple instability regions. These have also been observed in experiments, for example, by Chen & Jendrzejczyk (1983) and Andjelić *et al.* (1992). However, Païdoussis *et al.* (1995) have recently shown that damping and the existence of deviations of as little as 2% of a tube diameter from perfect array geometry can eliminate these multiple instability regions or make them very difficult to find. On the basis of their results, these latter authors argue that multiple instability regions are *practically* nonexistent. This position is reinforced by the theoretical work of Granger & Païdoussis (1995) which presents an important extension of previous theoretical models by deriving unsteady effects from the Navier-Stokes equations. The resulting ''quasi-unsteady'' model predicts no multiple instability regions. On comparison of their theoretical predictions with experiments for square-in line arrays, Granger & Païdoussis (1995) explain data which might be considered indicative of a secondary stability region as being due to vortex shedding. There is certainly no question that fluidelastic instability and vortex shedding exist as distinct excitation mechanisms and that these may overlap for tube arrays in water flows [see, for example, Weaver & Yeung, (1984) and Weaver & Fitzpatrick

(1988)]. With regard to perfect array geometry, this is virtually impossible to maintain for long flexible tubes with multiple supports. In spite of this, the multiple instability regions were readily detectable in the present study.

In an attempt to identify the excitation mechanism in the present case, Strouhal numbers were calculated for each of the response peak regions. Based on the upstream velocity at the peak, the Strouhal numbers are $0{\cdot}85 \pm 0{\cdot}1$, $1{\cdot}45 \pm 0{\cdot}2$ and $2{\cdot}4 \pm 0{\cdot}3$, from the highest to the lowest region respectively. The Strouhal number data summarized by Weaver & Fitzpatrick (1988) suggest a value in the range 1·1 to 1·5 while the more recent data of Chen (1993) gives a value closer to 1·7. Thus, the middle response region in the present study might be attributable to a vortex-shedding but the other two regions remain unexplained. However, with regard to a vortex-shedding explanation, it is important to note that careful pressure measurements, as discussed in Section 2, failed to indicate the presence of *any* constant Strouhal number phenomenon in the absence of tube motion. An interesting corroboration for this observation is provided by the flow visualization study of Price *et al.* (1995) for a parallel triangular array with a pitch ratio of 1·375. They observed no vortex shedding when the array was rigid but found a combination of vortex shedding and fluidelastic instability when one tube was flexible in the array. This points out the difficulty of attribution of excitation mechanism from flow visualization. Vortices will always be shed from an oscillating bluff body at the oscillation frequency but it cannot easily be determined whether the vortices are caused by, or are the cause of, the oscillations. If there are no periodic coherent vortex structures in the absence of structural motion, then the motion observed must be "fluidelastic" in the true sense of the word, i.e., elastic structural motion generates flow periodicity at the same frequency which becomes regenerative (self-excited) through mutual interaction. At least in this sense, the multiple response regions observed in the present study may be called "fluidelastic instability". Whether this fluidelastic mechanism is distinct from that producing very large amplitude damaging oscillations in heat exchanger tube arrays remains an open question.

It is also an open question as to whether, under different support arrangements, the amplitudes of vibration in the secondary instability regions will always be so small or will be incapable of generating damaging fretting wear. All of the data in the lower two stability regions correspond to modes higher than the first and, therefore, to higher frequencies. Thus, while the vibration amplitudes are very small, the local tube velocities and the modal energies are not. For example, the maximum tube velocity in test C (group 3, third mode, 285 Hz) is actually greater than that for the first mode at instability in test A (group 1, 12 Hz). Establishing criteria for fretting wear damage is beyond the scope of this paper. One thing is clear, the vibration amplitudes in the lower stability regions are small, and if maximum r.m.s. tube displacement is accepted as a valid criterion for tube damage, then the present results agree with the conclusions of Païdoussis *et al.* (1995), these lower instability regions are *practically* nonexistent.

4.3. Comparison with Empirical Design Criteria

The experimental data obtained were compared to the predictions of some commonly used empirical design correlations that follow equation (1) for uniform cross-flow or equation (3) for cross-flow with partial admission. These correlations are the ones proposed by Weaver & Fitzpatrick (1988), Pettigrew & Taylor (1991) and Au-Yang *et al.* (1991). All of them were obtained as safe stability boundaries of experimental data reported in the technical literature. Weaver & Fitzpatrick proposed different correlations for each of the four standard array geometries, whereas the other two design

TABLE 4
Parameters proposed to predict pitch critical velocities with equation (1)

Authors	Range	K	α
Au-Yang *et al.* (1991)	$\forall\ m\delta_W/(\rho d^2)$	4·0	0·5
Pettigrew & Taylor (1991)	$\forall\ m\delta_W/(\rho d^2)$	3·0	0·5
Weaver & Fitzpatrick (1988)	$m\delta_A/(\rho d^2) > 0{\cdot}3$	4·8	0·3
	$m\delta_A/(\rho d^2) < 0{\cdot}3$	1·0	0·0

criteria make no distinction. The corresponding K and α coefficients (for the parallel triangular array in the case of Weaver & Fitzpatrick's correlation) are summarized in Table 4.

Figure 15 presents the stability boundary corresponding to Weaver & Fitzpatrick (1988), who referred the mass-damping parameter to the measurements of damping in vacuum (air). For values of the mass-damping parameter less than 0·3, these authors established a constant critical pitch velocity equal to 1·0, which is remarkably close to the lower instability region shown by the data. Also, the value of 0·3 separating the ranges of the mass-damping parameter is nearly coincident with the upper limit of the secondary instability regions. Clearly, Weaver & Fitzpatrick's stability boundary fits the stability boundary obtained in this study very well.

Figure 16 presents the stability boundaries corresponding to the criteria proposed by Pettigrew & Taylor (1991) and Au-Yang *et al.* (1991), both of whom considered the values of damping measured in still fluid for the mass-damping parameter. Both of them assume in equation (1) an exponent $\alpha = 0{\cdot}5$ (Connors type) and so their stability boundaries are parallel straight lines in the log–log representation. If it is accepted that the maximum r.m.s. tube displacement must exceed something like 2% of a tube diameter to produce damaging fretting wear, then the criterion of Pettigrew & Taylor (1991) captures all of the significant instability points except point 5. While this point corresponds to a so-called "secondary" instability region, the vibration amplitudes reached 3·5% of a tube diameter, which is typically considered to be unacceptable. On the other hand, the criterion of Au-Yang *et al.* (1991), misses points 2, 3, 4, 5 and 11. All of these points correspond to unacceptably large vibration levels. It may be that these criteria are somewhat unconservative at low mass-damping parameters, especially that of Au-Yang *et al.* (1991), as a result of their having been established primarily on more idealized experiments with uniform flow over single span tubes.

5. CONCLUSIONS

An experimental study was conducted to determine the effects of nonuniform cross-flow on the stability behaviour of a tube array in the low mass-damping parameter range. Tests were conducted in a water tunnel on a parallel triangular tube array with a pitch-to-diameter ratio of 1·574 and cross-flow with partial admission (uniform flow over part of the tube length). Different natural frequencies and mode shapes were obtained by using a propped cantilever tube arrangement and moving the intermediate simple support (prop) along the tubes. Thus, the general configuration was 2-span tubes with boundary conditions fixed-pinned-free and flow across 30% of the tube length near the fixed end. The results are plotted on a stability map and compared with stability criteria from the literature. The principal conclusions are as follows.

1. The stability behaviour of multi-span tube arrays with a nonuniform liquid cross-flow is similar to that of a single span array subjected to uniform liquid cross-flow except that the critical mode depends on the flow distribution relative to the modal displacement along the tubes. At least for the range of parameters of the present study, this effect can be accounted for by using the energy fraction concept of previous studies.

2. The reduced velocity for fluidelastic instability in the critical mode is essentially independent of the mass-damping parameter at low values of this parameter. This agrees with earlier experimental results for uniform liquid flows across single-span tube arrays but contrasts with results for gas flows which show significant dependence on the mass-damping parameter.

3. The results of the present study suggest multiple regions of instability at low mass-damping parameters. These regions cannot simply be attributed to vortex-shedding resonance, as no periodic excitation at the appropriate Strouhal numbers could be measured on rigid tubes. However, at least in the present study, these lower regions of instability were associated with very small displacement amplitudes. If displacement amplitudes were to be taken as an acceptance criterion, these lower regions of instability may be considered as *practically* non-existent, in agreement with Païdoussis *et al.* (1995).

4. When the energy fraction for the critical mode is used in the mass-damping parameter, the empirical stability criterion presented by Weaver & Fitzpatrick (1988) fit the present data quite well. If the lower instability regions are ignored, the criterion of Pettigrew & Taylor (1991) also captures most of the present data.

ACKNOWLEDGEMENT

The authors gratefully acknowledge the financial support of the Fundación para el Fomento en Asturias de la Investigación Científica y la Tecnología (FICYT), Spain, under project number PB-TDI9605.

References

Andjelić, M. & Popp, K. 1989 Stability effects in a normal triangular cylinder array. *Journal of Fluids and Structures* **3,** 165–185.

Andjelić, M., Austermann, R. & Popp, K. 1992 Multiple stability boundaries of tubes in a normal triangular cylinder array. *ASME Journal of Pressure Vessel Technology* **114,** 336–343.

Au-Yang, M. K., Blevins, R. D. & Mulcahy, T. M. 1991 Flow-induced vibration analysis of tube bundles—A proposed Section III Appendix N non-mandatory code. *ASME Journal of Pressure Vessel Technology* **113,** 257–267.

Blevins, R. D. 1977 *Flow-Induced Vibration*. New York: Van Nostrand Reinhold.

Connors, H. J. 1970 Fluidelastic vibration of tube arrays excited by cross flows. In *Flow-Induced Vibration in Heat Exchangers* (ed. D. D. Reiff), pp. 42–56. New York: ASME.

Connors, H. J. 1978 Fluidelastic vibration of heat exchanger tube arrays. *ASME Journal of Mechanical Design* **100,** 347–353.

Chen, S. S. 1977 Dynamics of heat exchanger tube banks. *ASME Journal of Fluids Engineering* **99,** 462–469.

Chen, S. S. 1983 Instability mechanisms and stability criteria of a group of circular cylinders subject to cross flow. Part II: numerical results and discussion. *ASME Journal of Vibration, Acoustics, Stress and Reliability in Design* **105,** 253–260.

Chen, S. S. & Jendrzejczyk, A. 1983 Stability of tube arrays in cross-flow. *Nuclear Engineering and Design* **75,** 351–373.

Chen, Y. 1993 Strouhal periodicity in parallel triangular tube arrays. M. Eng. Thesis, Department of Mechanical Engineering, McMaster University, Ontario, Canada.

Franklin, R. B. & Soper, B. M. H. 1977 An investigation of fluidelastic instabilities in tube

banks subjected to cross flow. In *Proceedings 4th International Conference on Structural Mechanics in Reactor Technology (SMiRT)*, Paper No. F6/7.

GRANGER, S. & PAÏDOUSSIS, M. P. 1995 An improvement to the quasi-steady model with application to cross-flow induced vibration of tube arrays. In *Proceedings Sixth International Conference on Flow-Induced Vibration* (ed. P. W. Bearman), pp. 339–350. Rotterdam: Balkema. Also in *Journal of Fluid Mechanics* **320,** 163–184 (1996).

LEVER, J. H. & WEAVER, D. S. 1982 A theoretical model for fluidelastic instability in heat exchanger tube bundles. *ASME Journal of Pressure Vessel Technology* **104,** 147–158.

MORETTI, P. M. & LOWERY, R. L. 1976 Hydrodynamic inertia coefficients for a tube surrounded by rigid tubes. *ASME Journal of Pressure Vessel Technology* **98,** 190–193.

PAÏDOUSSIS, M. P. & PRICE, S. J. 1988 The mechanisms underlying flow induced instabilities of cylinder arrays in cross flows. *Journal of Fluid Mechanics* **187,** 45–59.

PAÏDOUSSIS, M. P., PRICE, S. J. & MUREITHI, N. W. 1995 On the practical nonexistence of multiple instability regions for heat exchanger arrays in cross-flow. In *Proceedings Sixth International Conference on Flow-Induced Vibration* (ed. P. W. Bearman), pp. 283–294. Rotterdam: Balkema. Also in *ASME Journal of Fluids Engineering* **118,** 103–109 (1996).

PARRONDO, J. L. 1992 Vibraciones fluidodinámicas en haces de cilindros bajo flujo cruzado: inestabilidad fluidoelástica. Tesis Doctoral, Departamento de Energía, Universidad de Oviedo, Gijón, Spain.

PARRONDO, J. L., EGUSQUIZA, E. & SANTOLARIA, C. 1993 Extension of the Lever & Weaver's unsteady analytical model to the fluidelastic instability of arrays of flexible cylinders. *Journal of Wind Engineering and Industrial Aerodynamics* **49,** 177–186.

PETTIGREW, M. J., SYLVESTER, Y. & CAMPAGNA, A. O. 1978 Vibration analysis of heat exchanger and steam generator designs. *Nuclear Engineering and Design* **48,** 97–115.

PETTIGREW, M. J. & TAYLOR, C. E. 1991 Fluidelastic instability of heat exchanger tube bundles: review and design recommendations. *ASME Journal of Pressure Vessel Technology* **113,** 242–256.

PRICE, S. J. 1995 A review of theoretical models for fluidelastic instability of cylinder arrays in cross flow. *Journal of Fluids and Structures* **9,** 463–518.

PRICE, S. J. & PAÏDOUSSIS, M. P. 1986 A single-flexible cylinder analysis for the fluidelastic instability of an array of flexible cylinders in cross-flow. *ASME Journal of Fluids Engineering* **108,** 193–199.

PRICE, S. J., PAÏDOUSSIS, M. P. & MARK, B. 1995 Flow-visualization of the interstitial cross-flow through parallel triangular and rotated square arrays of cylinders. *Journal of Sound and Vibration* **181,** 85–98.

WARING, L. F. & WEAVER, D. S. 1988 Partial admission effects on the stability of a heat exchanger tube array. *ASME Journal of Pressure Vessel Technology* **119,** 194–198.

WEAVER, D. S. & FITZPATRICK, J. A. 1988 A review of cross-flow induced vibration in heat exchanger tube arrays. *Journal of Fluids and Structures* **2,** 73–93.

WEAVER, D. S. & GOYDER, H. G. D. 1990 An experimental study of fluidelastic instability in a three-span tube array. *Journal of Fluids and Structures* **4,** 429–442.

WEAVER, D. S. & KOROYANNAKIS, D. 1982 A comparison of cross-flow induced vibration of a tube bundle in air and water. *ASME Journal of Pressure Vessel Technology* **104,** 139–146.

WEAVER, D. S. & PARRONDO, J. L. 1991 Fluidelastic instability in multispan heat exchanger tube arrays. *Journal of Fluids and Structures* **5,** 323–338.

WEAVER, D. S. & YEUNG, H. C. 1984 The effect of tube mass on the flow induced response of various tube arrays in water. *Journal of Sound and Vibration* **93,** 409–425.

APPENDIX: NOMENCLATURE

A	maximum amplitude of oscillation
C_M	added mass coefficient
d	diameter of tubes
f	frequency of vibration
f_A	natural frequency of tubes *in vacuo*
f_W	frequency of tubes in water
i	ith mode of vibration (subindex)
K	coefficient in equations (1), (2) and (3)
l	length of tubes

m	mass of tubes per unit length, added mass included
m_A	m with no added mass
MDE	mass-damping-energy fraction parameter, $m\delta/(\rho d^2 S_i)$
MDE_A	MDE with $\delta = \delta_A$
MDE_W	MDE with $\delta = \delta_W$
p	pitch of the array
S_i	energy fraction [equation (4)]
V	critical flow velocity
V_P	pitch critical flow velocity
V_U	upstream critical flow velocity
x	coordinate along tubes
α	exponent in equations (1) and (3)
δ	logarithmic decrement of damping
δ_A	δ of tubes in still air
δ_W	δ of tubes in still water
ρ	density of water
$\phi_i(x)$	shape function of tubes
$\psi(x)$	cross-flow distribution along tubes